Toward Reliable Algorithmic Self-Assembly of DNA Tiles: A Fixed-Width Cellular Automaton Pattern

ARTICLE *in* NANO LETTERS · AUGUST 2008

Impact Factor: 13.59 · DOI: 10.1021/nl0722830 · Source: PubMed

5 AUTHORS, INCLUDING:

Rizal F Hariadi
Harvard University
19 PUBLICATIONS **357** CITATIONS

NANO LETTERS

2007
Vol. 8, No. 7
1791-1797

Toward Reliable Algorithmic Self-Assembly of DNA Tiles: A Fixed-Width Cellular Automaton Pattern

Kenichi Fujibayashi,[†] Rizal Hariadi,[‡] Sung Ha Park,[§] Erik Winfree,[||,⊥] and Satoshi Murata*[,†]

Department of Computational Intelligence and Systems Science, Tokyo Institute of Technology, Midori-ku, Yokohama 226-8502, Japan, and Department of Applied Physics, Center for the Physics of Information, Department of Computation and Neural Systems, Department of Computer Science, California Institute of Technology, Pasadena, California 91125

Received September 7, 2007; Revised Manuscript Received October 10, 2007

ABSTRACT

Bottom-up fabrication of nanoscale structures relies on chemical processes to direct self-assembly. The complexity, precision, and yield achievable by a one-pot reaction are limited by our ability to encode assembly instructions into the molecules themselves. Nucleic acids provide a platform for investigating these issues, as molecular structure and intramolecular interactions can encode growth rules. Here, we use DNA tiles and DNA origami to grow crystals containing a cellular automaton pattern. In a one-pot annealing reaction, 250 DNA strands first assemble into a set of 10 free tile types and a seed structure, then the free tiles grow algorithmically from the seed according to the automaton rules. In our experiments, crystals grew to ~300 nm long, containing ~300 tiles with an initial assembly error rate of ~1.4% per tile. This work provides evidence that programmable molecular self-assembly may be sufficient to create a wide range of complex objects in one-pot reactions.

The Watson—Crick complementarity of DNA molecules allows one to design not only simple double-stranded helices but also complicated woven structures consisting of many DNA strands.[1] Well-designed structures will self-assemble during annealing from a high initial temperature at which point all molecules are single-stranded to a lower final temperature at which base-pairing is preferred. Complex sequences of assembly steps within such one-pot reactions may be achieved both thermodynamically, by ensuring that structures to be created in the initial steps have the highest melting temperatures, and kinetically, by controlling nucleation steps for molecular folding and crystal growth. Thermodynamic control has been used previously for two-step annealing wherein DNA "tiles" first form individually and then subsequently assemble into crystals as directed by complementary "sticky ends" that bind the tiles to each other.[2–6] Kinetic control also has been achieved using either scaffold strands[7,8] or seed structures.[9,10] Such control makes it possible to perform "algorithmic self-assembly", wherein matching rules encoded in the sticky-end sequences direct the development of a complex pattern.[11] Algorithmic self-assembly derives from Wang's mathematical investigation of the tiling problem,[12,13] which showed that the geometry of tiling can simulate Turing machines and their parallel-computation relatives, one-dimensional cellular automata. Similarly, algorithmic self-assembly of DNA tiles is Turing universal in principle.[11,14] However, previous demonstrations of algorithmic self-assembly had poor yield and high error rates,[8,15] bringing into question whether the complexity it promised theoretically could be achieved practically. In our experiments, crystals grew to ~300 nm long, containing ~300 tiles with an initial assembly error rate of ~1.4% per tile. To achieve this result, we modified the design of our DNA tiles to improve tile formation yield and demonstrated that boundary tiles can prevent aggregation and merging of growing crystals.

Results. ***A Cone-Shaped Assembly.*** In this work, our goal was to identify and minimize the major sources of errors and thus to establish a baseline for reliable and high yield algorithmic self-assembly in a one-pot reaction. The Sier-

* To whom correspondence should be addressed. E-mail: murata@dis.titech.ac.jp.
[†] Department of Computational Intelligence and Systems Science, Tokyo Institute of Technology.
[‡] Department of Applied Physics, California Institute of Technology.
[§] Center for the Physics of Information, California Institute of Technology.
[||] Department of Computation and Neural Systems, California Institute of Technology.
[⊥] Department of Computer Science, California Institute of Technology.

10.1021/nl0722830 CCC: $40.75
Published on Web 12/28/2007

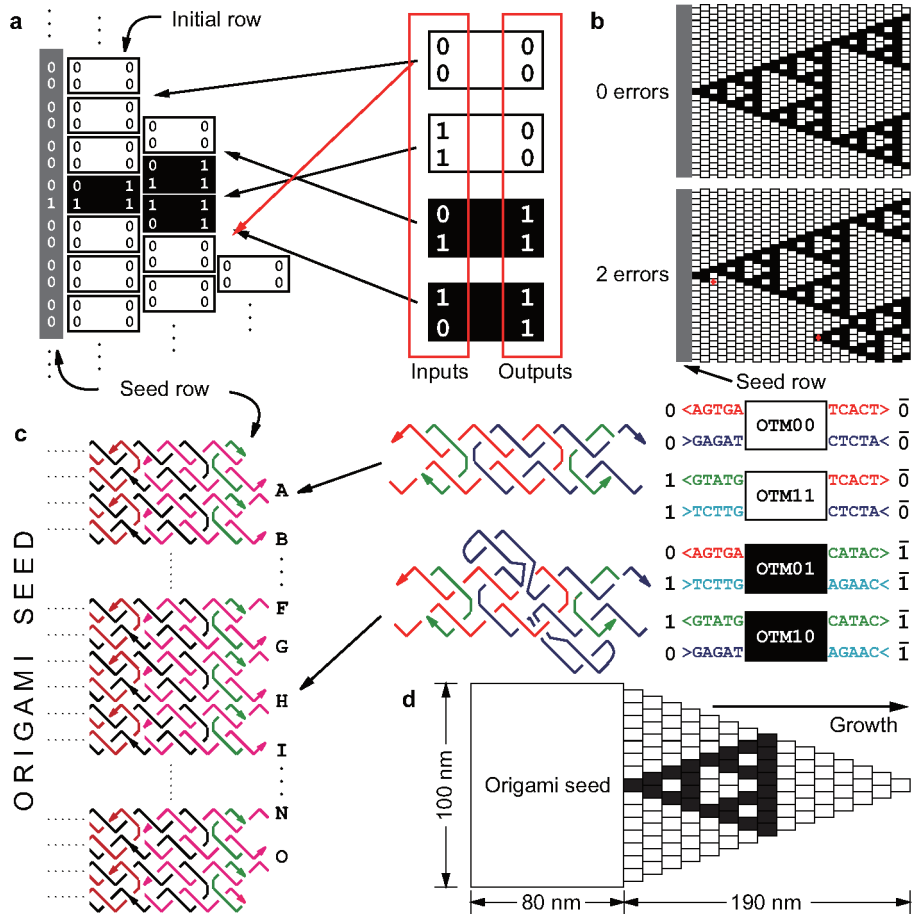

Figure 1. Logic of tile assembly for abstract tiles and DNA tiles. (a) Four abstract tiles that implement the XOR function ($0 \oplus 0 = 0$, $1 \oplus 1 = 0$, $0 \oplus 1 = 1$ and $1 \oplus 0 = 1$) during left-to-right growth. A "seed row" (the "0"th row) sets the boundary conditions for growth by specifying the initial row of tiles. Wherever both inputs match (black arrows), tiles may attach asynchronously to the seed row or to two adjacent tiles in the assembly. A single match (red arrow) is insufficient for attachment. Tiles are oriented and must be staggered (see Supporting Information, Figures S1, S2, and S5), so an incoming tile cannot make two matches to the same tile in the assembly. (b) When these assembly rules are executed without errors, these tiles grow from the seed row to produce the Sierpinski pattern (top). With errors (red tiles) the pattern is disrupted (bottom). A single error can result in a widespread change in the pattern, due to propagation of the incorrect information. (c) DNA implementation of the XOR tiles and structure of the DNA origami seed implementing the seed row. Each tile is of the DAO-E type;[11,17] in the modified motif variant used here, each tile is composed of two strands unique to that tile (red and dark blue) which contain 5-nt sticky ends whose sequence encodes the logical input and output for the tile, and two copies of the universal strut strand (green). Tiles that output "0" (OTM00 and OTM11) are called "0 tiles", while tiles that output "1" (OTM01 and OTM10) are called "1 tiles". (See Supporting Information, Figures S1 and S2 for details. "OTM" refers to the "original tile mechanism" of ref 16, in contrast to more advanced error reduction mechanisms such as those proposed in ref 23.) Odd and even locations use different sticky-end sequences to encode "0" and "1", ensuring proper staggering of the tiles during assembly. Tiles that output "1" have hairpin-forming subsequences that provide contrast for AFM imaging. The structure of the adapter tiles for the origami seed is shown at the left. The scaffold strand (black) and staple strands (brown) of the origami rectangle continue to the left and are not all shown. Each adapter tile is formed by a universal strut strand (green) and two adapter strands (magenta) containing subsequences specific to a location on the scaffold strand and the appropriate sticky ends for that location. (See Supporting Information, Figure S3 for the full structure of the origami seed and Figure S4 for sequences of the new adapter.) (d) The cone-shaped assembly produced by error-free growth from an origami seed specifying the initial row "0000000100000000". No further growth can occur unless insufficient attachments occur. See Supporting Information, Figure S5 for details.

pinski triangle was chosen as a test pattern because it requires only a small set of tiles yet it involves all the major assembly mechanisms in which errors could occur. Each tile "computes" the exclusive-or (XOR) function in the sense that a unique tile will bind at a site presenting a particular input pair (e.g., "0" and "1") and that this tile will present two outputs representing the XOR of the inputs (e.g., "1" and "1"; see Figure 1a). The logical constraint required for correct algorithmic growth is that a tile may attach only if it matches at least two inputs.[16] This is essential for growth of the correct pattern; errors may occur when a tile attaches by just one matching input (Figure 1b). In addition to the rules implemented by the tiles, it is necessary to provide initial conditions for the assembly; an initial row of "0"s with a single "1" will produce the Sierpinski triangle pattern. For molecular self-assembly, both the tiles and the initial conditions can be created using DNA structures (Figure 1c). Tiles use a double-crossover (DX) motif[17] that has been used previously for DNA tile-based self-assembly[2,8–10,15,18,19] but with two modifications (see Supporting Information, Figures S1 and S2): (i) sticky-ends are on the longer central strands rather than on the shorter peripheral strands, and (ii) the

shorter strands, lacking sticky ends, all have the same sequence and are called the "universal strut strand" (see Supporting Information, Methods). This reduces the number of strands required to create N tile types from $4N$ to $2N + 1$. In addition to reducing synthesis complexity, the universal strut motif improves the yield of tile formation, because only two strands must be adjusted to have comparable stoichiometry, while the universal strut strand can be in excess. To provide boundary condition information for the initial row, we use DNA origami[20] augmented with a layer of adapter tiles so that it can seed algorithmic growth[10] with modifications to account for the modified DX tile design. The origami seed self-assembles from a scaffold strand (7249-nt circular single-stranded DNA from the M13mp18 phage) as guided by 192 "staple strands", 32 "adapter strands", and 16 copies of the universal strut strand; the resulting rectangular structure presents 15 pairs of sticky ends (A through O) that may be programmed with arbitrary information by modifying the appropriate adapter strands (see Supporting Information, Figures S3 and S4). When the origami seed is programmed to present a single central "1", correct growth of the four XOR tiles on the seed results in a cone-shaped assembly with a small Sierpinski pattern (see Figure 1d and Supporting Information, Figure S5). Further growth can occur only if a tile binds to a single input, which is prohibited by the logical constraint required for algorithmic growth: a tile may bind only if it can attach by at least two sticky ends.[11,14,16]

In practice, however, perfect Sierpinski growth is difficult to achieve because several types of error may occur. For instance, a tile that has one or two mismatched inputs will usually only attach transiently to a growing crystal, but it could become permanently embedded if other tiles subsequently attached to it and grow around it. This kind of error is called a "growth error" and results in a disruption of pattern formation due to the incorporation and propagation of incorrect information (Figure 1b). Previous experiments on algorithmic self-assembly[8,15] reported growth error rates between $1-10\%$ per tile, although these estimates were imprecise due to highly variable crystal growth and selective imaging. A related second type of error results when a tile attaches by a single sticky end despite the absence of a tile to provide the other input and then gets locked in place by subsequent crystal growth. These are called facet nucleation errors.[18,21] A single facet nucleation error on a cone-shaped assembly (e.g., Figure 1d) would allow both forward and backward growth of an additional layer of tiles. These new tiles are also likely to contain and propagate incorrect information. The third type of error, a nucleation error, occurs when several tiles come together to form a small assembly that initiates further growth in the absence of the intended seed molecule. Lacking the correct boundary conditions, such assemblies tend to be ill-formed. Several methods for suppressing these three types of errors in DNA tile assembly have been proposed,[21–25] and experimental support for reducing facet, nucleation, and growth errors has been obtained.[9,18,19] Additionally, previous work has observed lattice defect errors, where the regular connectivity pattern of the tiles is disturbed locally.[2,8,15] In this work, we wished to simultaneously reduce all types of errors as a baseline for future work on more advanced methods of error suppression.[21–23,25]

Our initial experiments to grow cone-shaped Sierpinski assemblies from origami seeds established that the desired structure can form, but high assembly error rates prevented high yield synthesis. To demonstrate assembly of the cone shape irrespective of algorithmic pattern formation, we first created an origami seed containing a seed row of all "0"s (thus directing the initial row of DNA tiles to be "000000000000000") and annealed it together with just the OTM00 tile. Resulting structures were deposited on freshly cleaved mica and were imaged in solution using tapping mode atomic force microscopy (AFM). Although some cones did form, we were unable to prevent the formation of large crystals of the OTM00 tile in addition to the seed-nucleated assemblies (Figure 2a,b). Despite this concern, we prepared an origami seed that directs the initial row to be "000000010000000" and annealed it together with all four XOR tiles to observe full algorithmic self-assembly. In our first experiments the "1" tile often failed to attach at the central adapter, which could be explained by an energetic penalty (electrostatic or geometric) for attaching tiles that have hairpins (OTM01 and OTM10). In an attempt to counteract this effect, in subsequent cone-growth experiments we increased the nominal concentration of the OTM01 tile to 5 or 10 times higher than the other tiles. Although only roughly half of the origami seeds correctly nucleated the central "1" tiles, we were encouraged to find that in both cases, very few errors were observed within the 120 tiles of the cone area (see Figure 2c,d and Supporting Information, Figure S6). Because a perfect cone has stoichiometry [origami]:[OTM00]:[OTM11]:[OTM10]:[OTM01] = 1:80:13:13:14, while the experiment provided stoichiometry 1:50:50:50:250, after cones have grown we expect the OTM00 tile to be depleted and the other tiles to remain in excess, which can be expected to lead to many growth errors at that stage of assembly. Our greatest concern, however, was the prevalence of an error mode that we had not anticipated: multiple assemblies nucleated from distinct seeds appeared to have aggregated and merged. As even the best-separated assemblies showed signs of facet nucleation (growth beyond the ideal cone shape; see Supporting Information, Figure S6), we hypothesize that merging occurs when reverse growth from facet nucleation presents input sticky ends that then bind to the output of another assembly (see Supporting Information, Figure S7). We call this an aggregation and merging error. Notwithstanding these errors and much to our surprise, large correct Sierpinski patterns frequently arose within the V-shaped area between merged cone assemblies (Figure 2c,d). We also observed large correct Sierpinski patterns initiated by a single mismatch error within a large OTM00 patch (see Figure 2e and Supporting Information, Figure S8a,b). These Sierpinski triangles had fewer growth errors than any we had observed in previous systems,[8] which encouraged us to look for ways to reduce the dominant error mode, aggregation and merging.

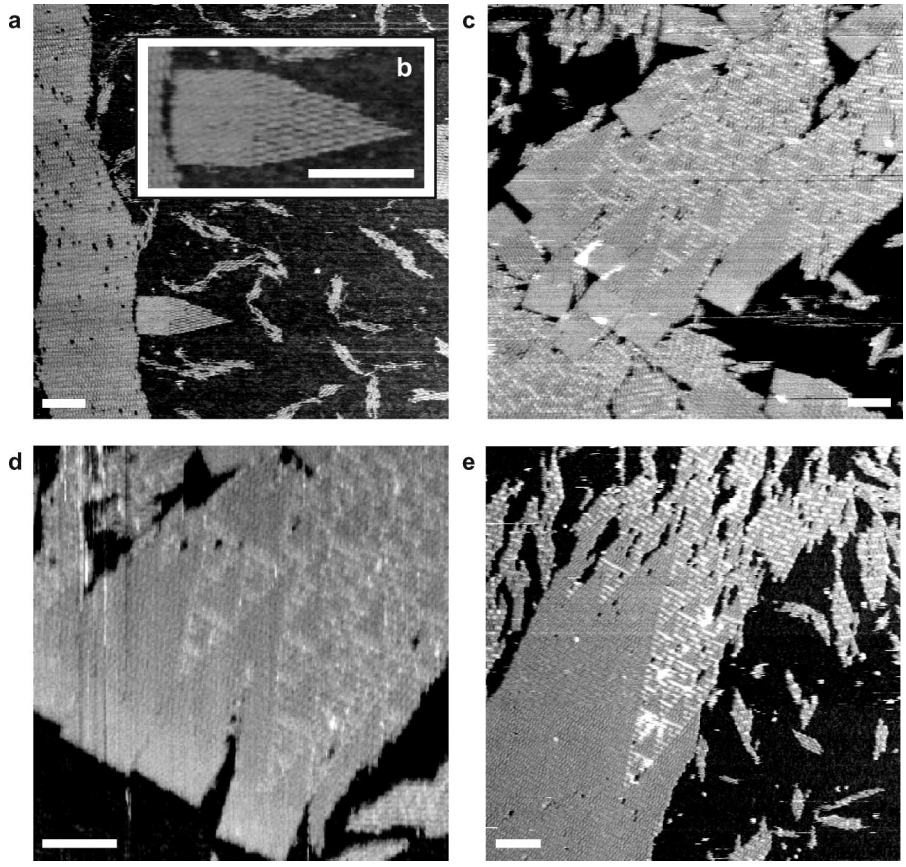

Figure 2. AFM images from cone-growth experiments. (a,b) Cones without patterns, grown using just OTM00 tiles and seeds presenting only "0". A large all "0" crystal (left) and a nearly perfect cone assembly. Holes in the large crystal are the result of damage during AFM imaging due to tip−sample interaction. Small poorly structured assemblies were also observed; these may have formed only at low temperatures from excess tiles in solution, or may be the result of crystal fragmentation during sample preparation for AFM imaging. [origami] = 1 nM, [OTM00] = 400 nM. Note that a perfect cone contains 120 OTM00 tiles, thus this experiment used an excess of tiles. However, experiments at a lower concentration (100 nM) produced only partially complete cones yet still contained large all "0" crystals, which motivated using the higher concentration. (c,d) Cones with patterns, grown using all four XOR tiles and seeds presenting a single central "1". Sierpinski patterns (with occasional errors) emerge both at the central "1" of origami seeds and at the sites of presumed aggregation and merging errors. [origami] = 1 nM, [OTM00] = [OTM11] = [OTM10] = 50 nM, [OTM01] = 250 nM. (e) A large Sierpinski pattern (with several errors) in a patch of OTM00 tiles. [origami] = 1 nM, [each XOR tile] = 100 nM. Scale bars are 100 nm.

A Ribbon Assembly. Reasoning that aggregation and merging will be reduced if sticky ends are exposed only at active growth fronts, we augmented the tile set so that crystals grow as fixed-width ribbons[9,10,19] by including "boundary tiles" that create an inert outer side (see Figure 3a and Supporting Information, Figure S9). The boundary tiles consist of two types of single tile (sT0 and sT1, or sT2 and sT3) and one type of the double tile (dT0 or dT1) for each side (see Figure 3b and Supporting Information, Figure S10). The motif of the single tiles is the same as that of OTM00 and OTM11, while the double tiles[9] each consist of two single tiles fused together at a hybridized sticky end with two other sticky ends made inert by converting them into hairpins. For the logic of pattern formation, the boundary tiles implement always "0" boundary conditions: following XOR rules, each single tile simply copies the information provided by its nonboundary tile input. To start the algorithmic self-assembly, we chose an initial row "0101010101-010", which results in a pattern with a 28-row period (see Figure 3a and Supporting Information, Figure S11). While logically each ribbon may grow indefinitely, in experiments the average ribbon length is determined by the ratio of concentrations of origami seeds, XOR tiles and boundary tiles.

Experiments to grow ribbons gave a high yield of structures with low error rates. First, we verified the formation of a patternless ribbon by using an origami seed specifying an initial row of 13 zeros flanked by the boundary and providing only the boundary tiles and OTM00 tiles in solution (Figure 4a). Correct-width ribbons grew from the origami seed. However, we also observed thinner spuriously nucleated ribbons with widths mostly less than six (see Supporting Information, Figure S12 for interpretations). Following previous work reducing nucleation errors,[9,10] we expected the origami seeds to nucleate Sierpinski-patterned ribbon growth at higher temperatures before significant amounts of spuriously nucleated structures can appear (see Supporting Information, Notes). Assuming that the thin ribbons formed from excess tiles at low temperatures and thus would not interfere with algorithmic growth at higher temperatures, we proceeded to attempt full algorithmic self-assembly of ribbons with the Sierpinski cellular automaton

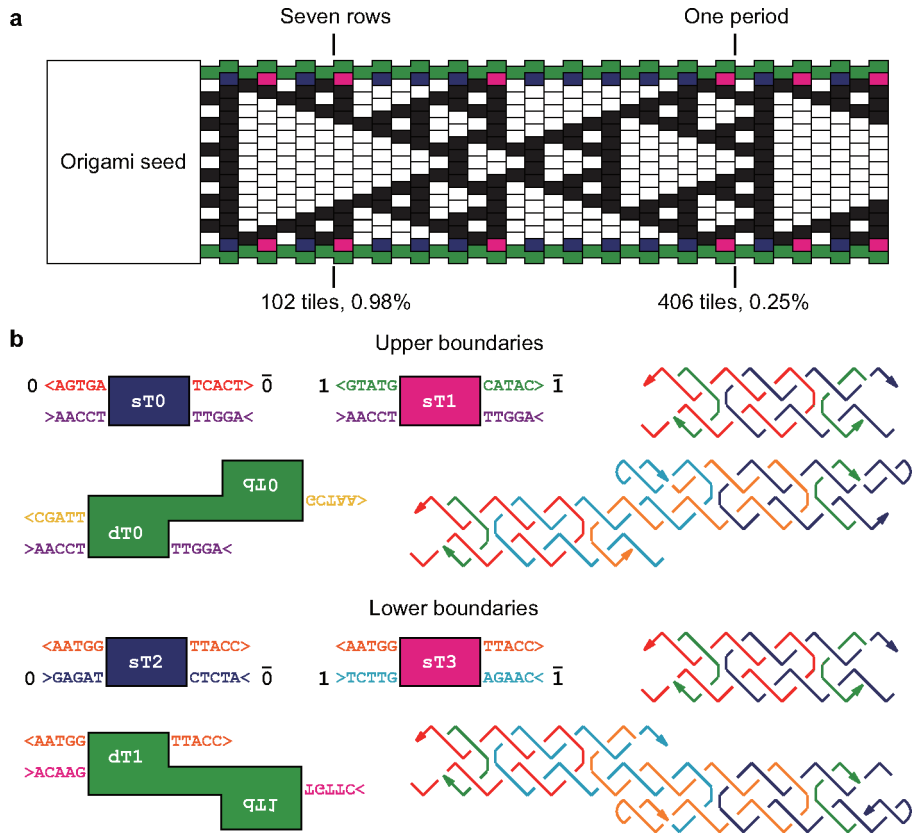

Figure 3. Logic of ribbon assembly. (a) The initial row "0101010101010" generates a pattern with period 28 rows, containing 406 tiles per repeat (14 each dT0, dT1; 10 each sT0, sT2; 4 each sT1, sT3; 68 each OTM01, OTM10, OTM11; 146 OTM00). Markings indicate the error rate corresponding to a single error within a given number of rows. (b) Boundary tile sticky-end logic and molecular motifs. Single tiles ("sT") are composed of two strands unique to the tile (red and dark blue) and two copies of the universal strut strand (green). Double tiles ("dT") are composed of four specific strands (red, light blue, orange, and dark blue) and two copies of the universal strut strand. See Supporting Information, Figure S10 for full sequences of boundary tiles and Figure S11 for sequences of the new adapter strands for the origami seed.

pattern, adjusting tile stoichiometry to more closely match usage in the ribbon. Typical fields of view showed that in fact most of the material formed into ribbons and merging of crystals was not observed despite common aggregation of the crystals (see Supporting Information, Figure S13). For analysis, we identified and imaged at high resolution 14 intact ribbon crystals that were well separated and maintained a correct constant width in their first 15 rows (see Supporting Information, Notes). With the aid of a program that displayed the logical consequences of errors, we deduced the locations of growth errors that explain the patterns on each crystal (see Figure 4b−e and Supporting Information, Figures S14 and S15). The highest error rate observed was 4.5% per tile; however, averaged over all crystals the error rate before the 15th row is only 1.4% (Figure 4h). The error rate increased, both in mean and in variance, after the 15th row, which could be due both to smaller sample size (not all crystals grew that long) and to stoichiometric disproportionation of the tile types during the assembly process. In addition to growth errors, we observed occasional lattice defect errors, which resulted in a decrease in the width of a ribbon (see Figure 4f,g and Supporting Information, Notes and Figure S16). Occasionally, large spuriously nucleated crystals were still observed, sometimes containing large Sierpinski patterns within an all-zero patch (see Supporting Information, Figure S8c,d).

Discussion. The Sierpinski-patterned ribbon assembly demonstrated here achieves a substantially lower error rate and higher yield of properly formed structures than both previously demonstrated algorithmic self-assembly experiments.[8,15] We think there are several possible reasons for this. First, because of the excellent control over nucleation provided by the DNA origami seeds, algorithmic crystal growth is likely to have occurred only slightly below the crystal's melting temperature in slightly supersaturated conditions that theoretically yield the lowest error rates. Second, because of the rigidity of the DNA origami seeds compared to the single-stranded scaffold strands used in prior work, there were fewer lattice defect errors (see Supporting Information, Notes). Third, here we used the DX tiles in a different orientation such that the input sticky ends are close to each other (left side sticky ends, this study) rather than far from each other (bottom sticky ends, previous studies). It is possible, though not proven, that this geometric difference could alter cooperativity or kinetics and reduce growth errors or lattice defect errors. Fourth, it initially seems remarkable that such low error rates are achieved despite the roughly 10-fold increase in number of strands required

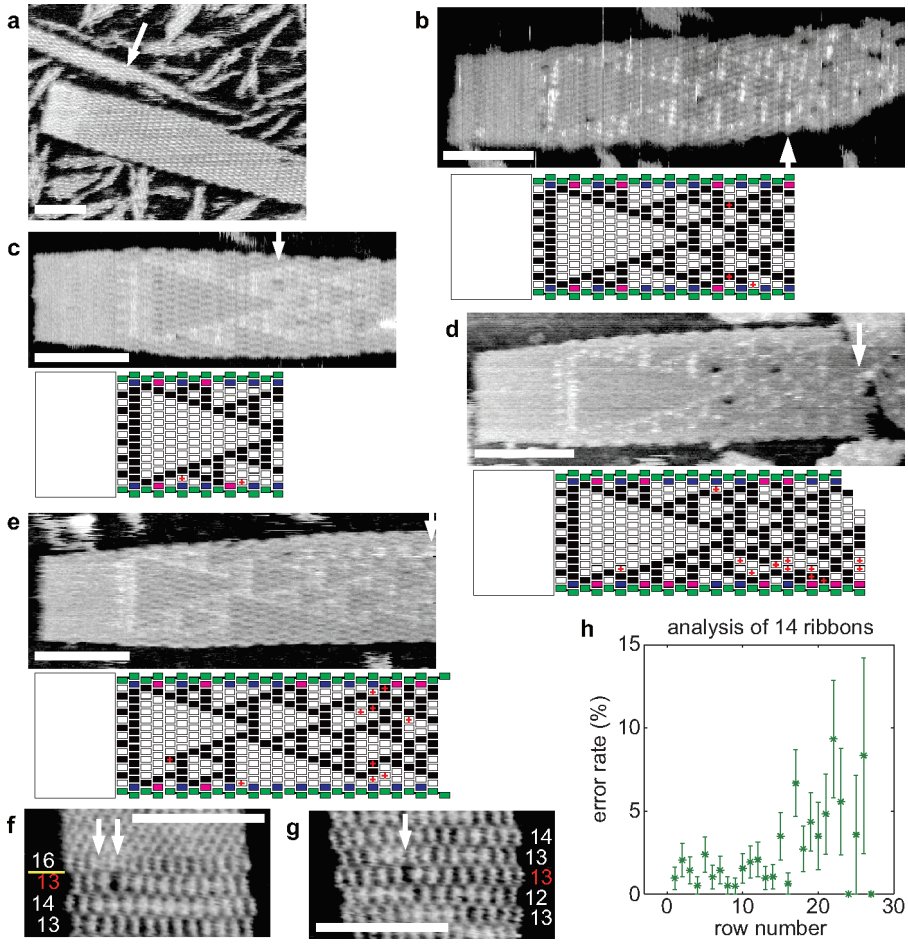

Figure 4. AFM images from ribbon-growth experiments. (a) Ribbons (without patterns) made of just OTM00 tiles flanked by boundary tiles. The white arrow indicates a spuriously nucleated width-4 ribbon. [origami] = 1 nM, [OTM00] = [each boundary tile] = 50 nM. All six boundary tiles were used, even though only half of them are required for the all "0" ribbon. We obtained longer correct-width ribbons by increasing the concentration of boundary tiles, but at the same time the number of thinner ribbons increased (data not shown). (b−e) Ribbons (with patterns) using all XOR tiles. Below each image is our interpretation of a constant-width portion with error tiles indicated with a red "plus". Arrows indicate where analysis stopped due to a change in width. (f,g) Zoom of a ribbon with lattice defect errors (also shown in Supporting Information, Figure S16). High-amplitude tapping during AFM produced images in which individual tiles are clear but hairpins cannot be distinguished. Numbers at the left indicate how many tiles are in each row. The seed row has 16 adapter tiles (above the yellow line). The lattice defect errors in (f) occurs in the initial row, the most common location for lattice defect errors. The arrow in (g) indicates a lattice defect error at the 18th row (during growth). [origami] = 1 nM, [each XOR tile] = 50 nM, [each boundary tile] = 10 nM. Depletion of the OTM00 tiles is expected to occur after ribbons have grown to an average length of 10 layers (see Supporting Information, Figure S9). (h) Plot of the fraction of erroneous tiles as a function of the distance from the origami seed. Error bars indicate standard deviation. Scale bars in the images are 100 nm.

for the origami seed, which could interfere with tile formation and assembly due to spurious interactions between strands; however, near the crystal melting temperature, where we think seeded growth occurs, thermodynamically stable bimolecular interactions must involve roughly ten or more base pairs, which is unlikely for random sequences.

Nonetheless, several opportunities for further improvements became apparent during this work. First, optimizing tile and seed concentrations and relative stoichiometry was difficult; the apparent energetic cost of incorporating tiles containing hairpins for AFM contrast caused us to increase the concentration of such tiles 5- or 10-fold, further exacerbating the disproportionation of tile types in solution. Ameliorating disproportionation is particularly challenging for algorithmic self-assembly in a one-pot reaction because the rate of free tile consumption is typically unequal for the different tile types and furthermore varies from row to row in potentially complex ways.[26] A homeostasis mechanism to hold the tile concentrations constant during assembly, whether endogenous or controlled externally by microfluidics,[27] would significantly improve the assembly process. Additionally, an alternative to DNA hairpins for labeling individual tiles with high yield would help make energetics nearly equal for all tile types. Second, the swelling that occurs between the tightly woven origami seed and the tile-based ribbon crystal (see Supporting Information, Notes) indicates that nucleation is inhibited by a lattice-spacing mismatch; a redesigned seed could ameliorate this effect, improving nucleation and thus allowing algorithmic growth to proceed even closer to the crystal's melting temperature. In summary, demonstrating algorithmic self-assembly within a programmably nucleated finite-width ribbon has advanced our understanding and ability to control the thermodynamics and

kinetics of multistage self-assembly processes in one-pot reactions.

Methods. ***Sample Preparation.*** All strands for tiles were synthesized and PAGE purified by Integrated DNA Technologies (Coralville, IA). Concentrations were measured based on absorbance at 260 nm in water and standard sequence-dependent extinction coefficients. Thus, all concentrations reported here are nominal and more so for tiles and origami whose yields were not precisely measured. For each single tile, strands were mixed in the ratio [universal strut strand]:[each tile strand] = 3:1, and for each double tile, strands were mixed in the ratio [universal strut strand]:[each tile strand] = 6:1. Because each XOR tile requires 2 universal strut strands and 2 tile-specific strands, this results in an excess of universal strut strands in solution. We call this a "tile mix". Staple strands for the "tall, thin" rectangular DNA origami are exactly as in the original work,[20] except that no staple strands contained dumbbell-hairpins and the staples on the left and right sides were omitted, that is, of the 224 original staple strands, we used 192. Staple strands and adapter strands were not purified. The concentration ratio among the M13mp18 strand, staple strands, adapter strands, and universal strut strand is 1:4:4:(4 × 16). This is called the "origami mix". For any given experiment, the origami mix and the relevant tile mixes are combined such that the nominal concentrations of the M13mp18 strand and of each tile-specific strand are as stated.

Annealing Protocols. All strands comprising each tile and the origami seed were mixed in TAE/Mg^{2+} buffer (40 mM Tris-Acetate, 1 mM Na_2 EDTA, 12.5 mM Mg Acetate). For samples in Figure 2 and Supporting Information, Figure S8a,b, we annealed samples using an Eppendorf Mastercycler. Temperature was decreased in stages: (1) kept at 90 °C for 10 min, (2) linearly decreased from 90 to 40 °C during 50 min, (3) linearly decreased from 40 to 25 °C during 15 h. Other samples were annealed in a hot water bath (2 L) contained in a Styrofoam box. In this case, temperature was exponentially decreased from 95 °C to room temperature during 50 h, with a half-time of roughly 10 h.

AFM Imaging. After self-assembly was complete, 5 μL of sample was deposited on freshly cleaved mica, followed by an additional 40 μL of buffer. AFM imaging was performed on a Digital Instruments Nanoscope III (Veeco Metrology, Santa Barbara, CA) using fluid-tapping mode in TAE/Mg^{2+} buffer, as described previously.[8,20]

DNA Sequence Design. All DNA sequences except for the M13mp18 strand and the 192 staple strands were designed as described previously[2,8,9] using programs written in MATLAB, available at http://www.dna.caltech.edu/DNAdesign/. Sequences are optimized so that the number of undesired subsequences that exactly match another subsequence is minimized and the predicted binding energies of sticky-end pairs were matched. See Supporting Information, Methods for sequences.

Acknowledgment. This work was supported by Grant-in-Aid for Scientific Research on Priority Areas (No. 17059001) from MEXT and Grant-in-Aid for Scientific Research (A) (No. 19200023) from JSPS to S.M., JSPS Research Fellowships for Young Scientists (No. 05697) to K.F., with additional support from NSF Grants (Nos. 0432193, 0093486) to E.W., and a Center for the Physics of Information postdoctoral fellowship to S.H.P.

Supporting Information Available: Supplementary notes, methods, and figures. This material is available free of charge via the Internet at http://pubs.acs.org.

References

(1) Seeman, N. C. *Int. J. Nanotech.* **2005**, *2*, 348–370.
(2) Winfree, E.; Liu, F.; Wenzler, L. A.; Seeman, N. C. *Nature* **1998**, *394*, 539–544.
(3) Mao, C.; Sun, W.; Seeman, N. C. *J. Am. Chem. Soc.* **1999**, *121*, 5437–5443.
(4) LaBean, T. H.; Yan, H.; Kopatsch, J.; Liu, F.; Winfree, E.; Reif, J. H.; Seeman, N. C. *J. Am. Chem. Soc.* **2000**, *122*, 1848–1860.
(5) Yan, H.; Park, S. H.; Finkelstein, G.; Reif, J. H.; LaBean, T. H. *Science* **2003**, *301*, 1882–1884.
(6) He, Y.; Chen, Y.; Liu, H.; Ribbe, A. E.; Mao, C. *J. Am. Chem. Soc.* **2005**, *127*, 12202–12203.
(7) Yan, H.; LaBean, T. H.; Feng, L.; Reif, J. H. *Proc. Natl. Acad. Sci. U.S.A.* **2003**, *100*, 8103–8108.
(8) Rothemund, P. W. K.; Papadakis, N.; Winfree, E. *PLoS Biol.* **2004**, *2*, 2041–2053.
(9) Schulman, R.; Winfree, E. *Proc. Natl. Acad. Sci. U.S.A.* **2007**, *104*, 15236–15241.
(10) Barish, R. D. Personal communication, 2007.
(11) Winfree, E. On the computational power of DNA annealing and ligation. In *DNA Based Computers*, Vol. DIMACS 27; Lipton, R. J., Baum, E. B., Eds.; AMS Press: Providence, RI, 1996.
(12) Wang, H. *Bell Syst. Tech. J.* **1961**, *40*, 1–42.
(13) Wang, H. Dominoes and the AEA case of the decision problem. In *Proceedings of the Symposium on the Mathematical Theory of Automata*; Fox, J., Ed.; Polytechnic Press: Brooklyn, NY, 1963.
(14) Winfree, E.; Yang, X.; Seeman, N. C. Universal computation via self-assembly of DNA: Some theory and experiments. In *DNA Based Computers II*, Vol. DIMACS 44; Landweber, L. F., Baum, E. B., Eds.; AMS Press: Providence, RI, 1998.
(15) Barish, R. D.; Rothemund, P. W. K.; Winfree, E. *Nano Lett.* **2005**, *5*, 2586–2592.
(16) Winfree, E. Simulations of computing by self-assembly. Caltech CS-TR:1998.22; Caltech: Pasadena, CA, 1998.
(17) Fu, T.-J.; Seeman, N. C. *Biochemistry* **1993**, *32*, 3211–3220.
(18) Chen, H.-L.; Schulman, R.; Goel, A.; Winfree, E. *Nano Lett.* **2007**, *7*, 2913–2919.
(19) Park, S. H. Personal communication, 2007.
(20) Rothemund, P. W. K. *Nature* **2006**, *440*, 297–302.
(21) Chen, H.-L.; Goel, A. Error free self-assembly using error prone tiles. In *DNA Computing 10*, Vol. LNCS 3384; Ferretti, C., Mauri, G., Zandron, C., Eds.; Springer-Verlag: Berlin and Heidelberg, 2005.
(22) Winfree, E.; Bekbolatov, R. Proofreading tile sets: Error correction for algorithmic self-assembly. In *DNA Computing 9*, Vol. LNCS 2943; Chen, J., Reif, J. H., Eds.; Springer-Verlag: Berlin and Heidelberg, 2004.
(23) Fujibayashi, K.; Murata, S. A method of error suppression for self-assembling DNA tiles. In *DNA Computing 10*, Vol. LNCS 3384; Ferretti, C., Mauri, G., Zandron, C., Eds.; Springer-Verlag: Berlin and Heidelberg, 2005.
(24) Schulman, R.; Winfree, E. Programmable control of nucleation for algorithmic self-assembly. In *DNA Computing 10*, Vol. LNCS 3384; Ferretti, C., Mauri, G., Zandron, C., Eds.; Springer-Verlag: Berlin and Heidelberg, 2005. Extended abstract in *DNA Computing 10*; preprint of the full paper is cond-mat/0607317 on arXiv.org.
(25) Reif, J. H.; Sahu, S.; Yin, P. Compact error-resilient computational DNA tiling assemblies. In *DNA Computing 10*, Vol. LNCS 3384; Ferretti, C., Mauri, G., Zandron, C., Eds.; Springer-Verlag: Berlin and Heidelberg, 2005.
(26) Wolfram, S. *A New Kind of Science*; Wolfram Media: Champaign, IL, 2002; pp 255−260.
(27) Somei, K.; Kaneda, S.; Fujii, T.; Murata, S. A microfluidic device for DNA tile self-assembly. In *DNA Computing 11*, Vol. LNCS 3892; Carbone, A., Pierce, N. A., Eds.; Springer-Verlag: Berlin and Heidelberg, 2006.

NL0722830